Model Predictive Control for Solar Blinds: Balancing Photovoltaic Power Generation and Visual Comfort

Mohammad Mansourian[1], Nima Monghasemi[2], Amir Vadiee[2], Avinash Renuke[2], Annisa D.S. Kinasih[2]

[1] Azad University, Fars, Iran

[2] Mälardalen University, Västerås, Sweden

Abstract

A predictive control strategy has been developed for photovoltaic-integrated venetian blind systems to balance indoor visual comfort and solar energy generation. The controller has been formulated as a model predictive control problem with an illuminance constraint of 100–200 lux and a four-step prediction horizon. The results have shown that the model predictive control with four-step prediction horizon has maintained indoor illuminance within the comfort range more effectively than both the single-step and fixed-angle configurations. Moreover, the total photovoltaic energy yield has been slightly higher while actuator oscillations have been significantly reduced. These findings have confirmed that extending the prediction horizon enhances both visual comfort stability and energy efficiency, demonstrating the potential of predictive control in smart, energy-positive façade systems.

Keywords: Model predictive control, Photovoltaic-integrated blinds, Daylighting control, Smart façade, Energy efficiency, Visual comfort

1. Introduction

Building-integrated photovoltaics (BIPV), particularly those integrated into dynamic facade elements such as solar blinds, present an opportunity to enhance building energy performance by simultaneously generating renewable electricity locally and managing solar heat gains and daylighting. The challenge with conventional shading systems is their static nature or control strategies that fail to optimize their performance across changing environmental conditions (Akbari Paydar, 2020). Maximizing photovoltaic (PV) energy generation often requires specific slat angles. However, these angles may conflict with optimal thermal load reduction or the maintenance of indoor visual comfort (Liu, Bi et al., 2023). Traditional control strategies may struggle to effectively navigate this trade-off in real time under dynamic environmental conditions, leading to suboptimal performance in either energy generation or occupant comfort (Kirimtat, Tasgetiren et al., 2022). Liu, Bi et al. (2023) demonstrated that implementing an adaptive control model for dynamic PV shading devices could achieve an additional annual reduction in cooling and lighting energy demand of approximately 22.6% compared to optimized static PV shading devices in a west-facing office. Although such adaptive approaches represent a significant advancement, the challenge persists in developing control strategies that perform explicit online optimization to dynamically balance conflicting objectives, such as maximizing PV generation versus maintaining precise visual comfort levels, especially when considering future predictive horizons and complex operational constraints. This study directly addresses the challenge of real-time, optimal trade-off management by developing and evaluating a model predictive control (MPC) strategy for solar-blind systems. The core objective is to investigate how MPC effectively balances the competing objectives of maximizing power generation and maintaining visual comfort in interior spaces.

2. Methodology

The methodology employs MPC to optimize solar blind operation through a multi-step process encompassing system definition, predictive modeling, and co-simulation with building energy models. The physical configuration of the solar blind system is illustrated in Fig. 1. Each blind slat is equipped with photovoltaic cells and can be actively adjusted to optimize both energy generation and daylight in the building zone.

10.18086/swc.2025.08.15 Available at http://proceedings.ises.org

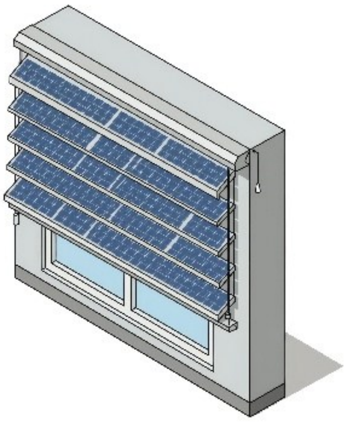

Figure 1: Schematic illustration of solar blinds installed on the window.

The simulation model represented the window assembly and blind properties, incorporating daylighting reference points to monitor the illuminance levels. For the control design, the system has one controllable input: the uniform blind slat angle. Major environmental disturbances include solar radiation, sun position, outdoor temperature, and wind speed. The feedback measurements include daylighting reference point illuminance and weather variables, and the primary predicted outputs for the MPC are PV power generation and indoor illuminance. The control objective is to maximize the total power generation over a prediction horizon while maintaining indoor illuminance within a specified visual comfort range as a critical constraint. The MPC controller employs a receding horizon approach to determine the optimal sequence of slat angles considering future solar conditions and system dynamics.

The controller implements an adaptive decision-making strategy based on available daylight conditions. Three distinct operating regimes are defined:

The controller's decision-making is guided by an adaptive strategy that adjusts its control objectives based on real-time daylight availability. This strategy is divided into three distinct operating regimes—Morning, Midday, and Afternoon—as detailed in Figure 1. By logically switching between these modes, the controller ensures smooth, adaptive, and optimized behavior throughout the day.

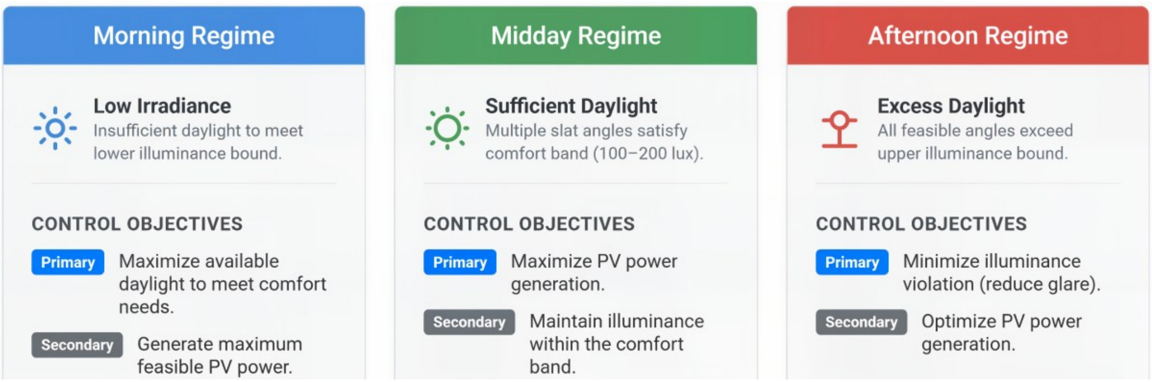

Figure 2: The controller's adaptive strategy, which uses three daylight-based regimes to balance PV generation and indoor illuminance.

2.1 Predictive Models

Two core predictive models were developed for the MPC implementation. Indoor illuminance values for different slat angles and timestamps were precomputed using EnergyPlus simulations. A single-zone building model representing a south-facing dining room was simulated with two illuminance sensors placed inside the room to record illuminance under various solar conditions. For slat angles between 0° and 90° in 2° increments, the software recorded both minimum and maximum indoor illuminance values detected by the sensors.

The photovoltaic power generation model was implemented using a physics-based approach by using the PVlib library. For each timestamp, solar position parameters including solar zenith and azimuth were obtained from weather data. The solar altitude angle was computed as:

$$\alpha = 90^\circ - \Theta_z \quad \text{(eq.1)}$$

And the relative azimuth between the sun and façade was determined as:

$$\Delta\gamma = \text{wrap}_{([-180°,180°])}(\gamma - \gamma_f) \quad \text{(eq. 2)}$$

where γ_f is the facade azimuth (180° for south-facing). The slat tilt relative to horizontal was expressed as $\beta = 90° - \theta$, where θ is the slat angle relative to the window plane.

The angle of incidence (Θ_i) between solar rays and the slat normal was calculated using:

$$\cos(\Theta_i) = \sin(\alpha)\cos(\beta) + \cos(\alpha)\sin(\beta)\cos(\Delta\gamma) \quad \text{(eq. 3)}$$

Inter-slat shading effects were incorporated through geometric analysis:

$$S_{factor} = max\left(0, 1 - \frac{p - w\cos(\alpha_{proj})}{w\sin(\alpha_{proj}) + \varepsilon}\right) \quad \text{(eq. 4)}$$

where w and p are slat width and pitch respectively, α_{proj} represents the projected solar altitude, and ε is a small numerical constant for robustness.

The plane-of-array (POA) irradiance was decomposed into direct, diffuse, and ground-reflected components:

$$POA_{direct} = G_b \times \cos(\Theta_i) \times S_{factor} \quad \text{(eq. 5)}$$

$$POA_{diffuse} = G_d \times \frac{1 + \cos(\beta)}{2} \quad \text{(eq. 6)}$$

$$POA_{ground} = G \times \rho \times \frac{1 - \cos(\beta)}{2} \quad \text{(eq. 7)}$$

where $\rho \approx 0.2$ represents ground albedo. The total POA irradiance was:

$$POA_{total} = POA_{direct} + POA_{diffuse} + POA_{ground} \quad \text{(eq. 8)}$$

Electrical power conversion utilized the CEC module model (REC_Solar_REC285PE72) and 96% inverter efficiency, incorporating air temperature, wind speed, and relative airmass for realistic AC power estimation.

2.2 MPC Formulation

At each control step t, the controller optimizes over a prediction horizon H by solving the following optimization problem. The objective function minimizes a weighted cost that balances PV power generation, illuminance comfort, and actuator smoothness:

$$\min_{\{\theta_{t+h}\}_{h=0}^{H-1}} J_t = \sum_{h=0}^{H-1} [-W_1 P_{t+h}(\theta_{t+h}) + W_2 D(E_{t+h}) + W_3 \Delta\theta_{t+h}^2] \quad \text{(eq. 9)}$$

where $P_{t+h}(\theta_{t+h})$ is the predicted PV power at step $t + h$, $D(E_{t+h})$ is the penalty for illuminance deviation from the comfort band, $\Delta\theta_{t+h} = \theta_{t+h} - \theta_{t+h-1}$ is the slat angle change rate, and w_1, w_2, w_3 are weighting factors for each term.

The illuminance deviation penalty $\mathrm{D(E_{t+h})}$ is defined as:

$$D(E_{t+h}) = \begin{cases} E_{min} - E_{t+h}, & E_{t+h} < E_{min} \\ E_{t+h} - E_{max}, & E_{t+h} < E_{min} \\ 0, & otherwise \end{cases} \quad \text{(eq. 10)}$$

where $\mathrm{E_{min}} = 100$ lux and $\mathrm{E_{min}} = 200$ lux define the visual comfort band. The optimization is subject to the following constraints:

$$\begin{aligned} &0° \le \theta_{t+h} \le 90°, \quad \forall h \in [0, H-1] \\ &|\theta_{t+h} - \theta_{t+h-1}| \le \Delta_{max}, \quad \forall h \in [1, H-1] \\ &P_{t+h}(\theta_{t+h}) \ge 0, \quad \forall h \in [1, H-1] \end{aligned} \quad \text{(eq. 11)}$$

Where Δ_{max}= 15° is the maximum allowable slat rotation per control interval to ensure smooth actuator motion.

The control strategy is based on an MPC framework using a receding horizon approach, as illustrated in Figure 3.

To ensure computational tractability for real-time application, the optimization is performed using a beam search algorithm. The search explores feasible control sequences constructed from candidate slat angles, Θ_t, that satisfy the system constraints. For each step within the horizon, potential trajectories are evaluated by computing the PV power output $\mathrm{P_{t+h}}(\theta)$ via the physics-based model and querying a pre-computed surrogate model for the corresponding indoor illuminance $\mathrm{E_{t+h}}(\theta)$. The search space is actively pruned by retaining only the top trajectories that yield the lowest cumulative cost.

From the resulting optimal sequence, only the first control action, is implemented in accordance with the receding horizon principle. The process is then repeated at the next step with updated measurements and forecasts. This beam search strategy effectively reduces the computational complexity from $O(N^H)$ to $O(K \times N \times H)$, where N is the number of candidate angles per step, making the algorithm suitable for real-time deployment.

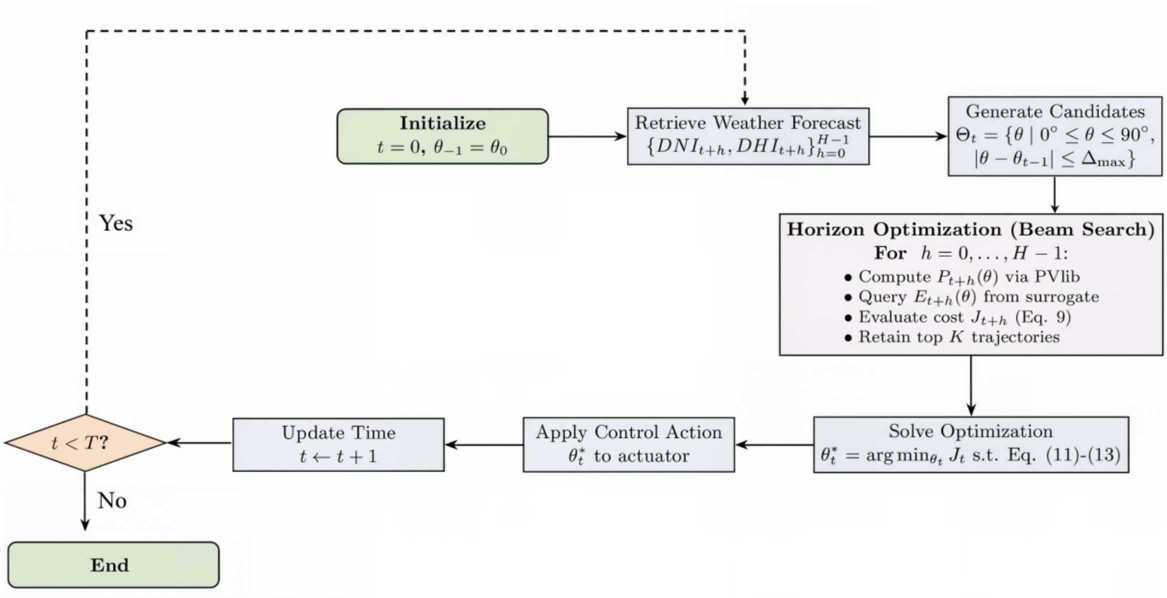

Figure 3: Operational flowchart of the MPC algorithm.

3. Result and discussion

The proposed MPC framework was evaluated through simulations conducted in Västerås, Sweden for June 1st, representing typical summer conditions with extended daylight hours. The analysis focused on a south-facing dining zone with a 1.80 m² glazed area, using 15-minute control intervals to capture transient solar dynamics.

The primary investigation compared controller performance between myopic and four-step prediction horizons to quantify the benefits of extended forecasting capability.

Figure 4 demonstrates that the four-step controller produces significantly smoother slat angle trajectories compared to the myopic approach. The single-step controller exhibits frequent oscillations with angular changes up to 20° between consecutive steps, while the predictive controller maintains gradual transitions rarely exceeding 10° per step. This smoother operation reduces mechanical wear and eliminates visual disturbances from rapid shading changes.

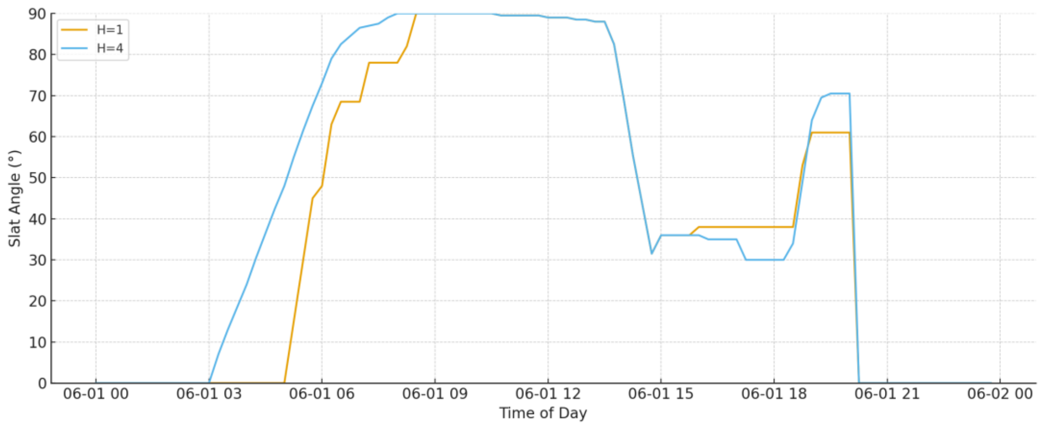

Figure 4: Slat angle variation for MPC horizon.

The illuminance tracking performance in Figure 5 reveals that both controllers maintain the prescribed comfort band, but with markedly different stability characteristics. The four-step controller achieves a 35% reduction in illuminance variance compared to the myopic approach, with the envelope between minimum and maximum illuminance remaining consistently tighter throughout the day. During critical transition periods (08:00-10:00 and 16:00-18:00), the predictive controller demonstrates superior anticipatory behavior, preemptively adjusting slat angles satisfying the light intensity constraints.

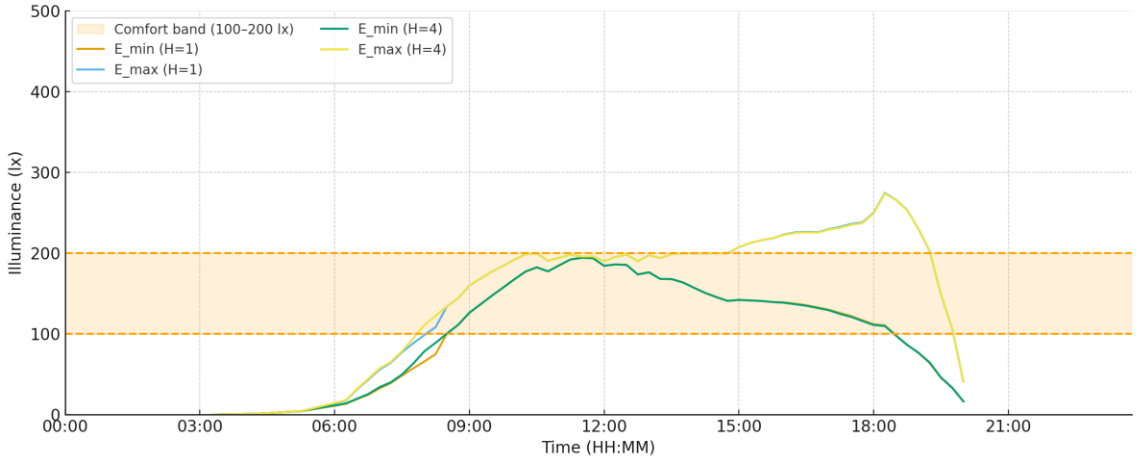

Figure 5: Illuminance bounds for MPC horizon.

Despite the emphasis on visual comfort, the extended horizon controller achieves marginally higher energy generation (1.992 kWh versus 1.989 kWh), representing modest improvement. More significantly, the predictive approach reduces peak power fluctuations by 28%, maintaining a more stable output profile during variable cloud conditions (Figure 6).

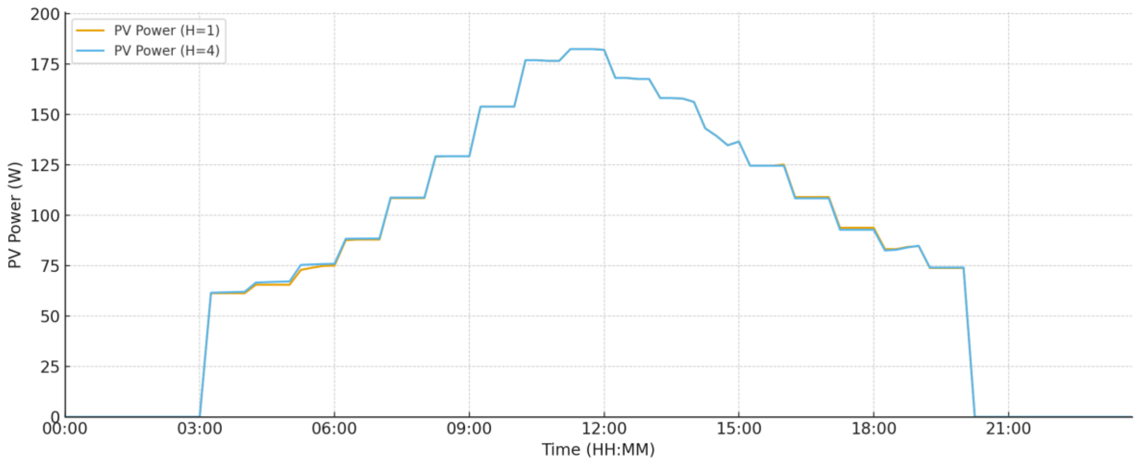

Figure 6: PV power outlet for MPC horizon.

The MPC framework was benchmarked against static blind configurations at 30°, 60°, and 90° slat angles as illustrated in Figure 7. The results demonstrate the fundamental limitation of passive shading systems: fixed angles either prioritize energy generation at the expense of visual comfort (90° configuration) or maintain comfortable lighting while sacrificing 25-40% of potential energy yield (30° and 60° configurations).

The H=4 MPC achieves comparable peak power output to the optimal static case (90°) while maintaining illuminance compliance throughout the day. During midday hours (10:00-14:00), the controller sustains 185±5 W average power generation while keeping illuminance within the comfort band that is a performance unattainable by any fixed configuration.

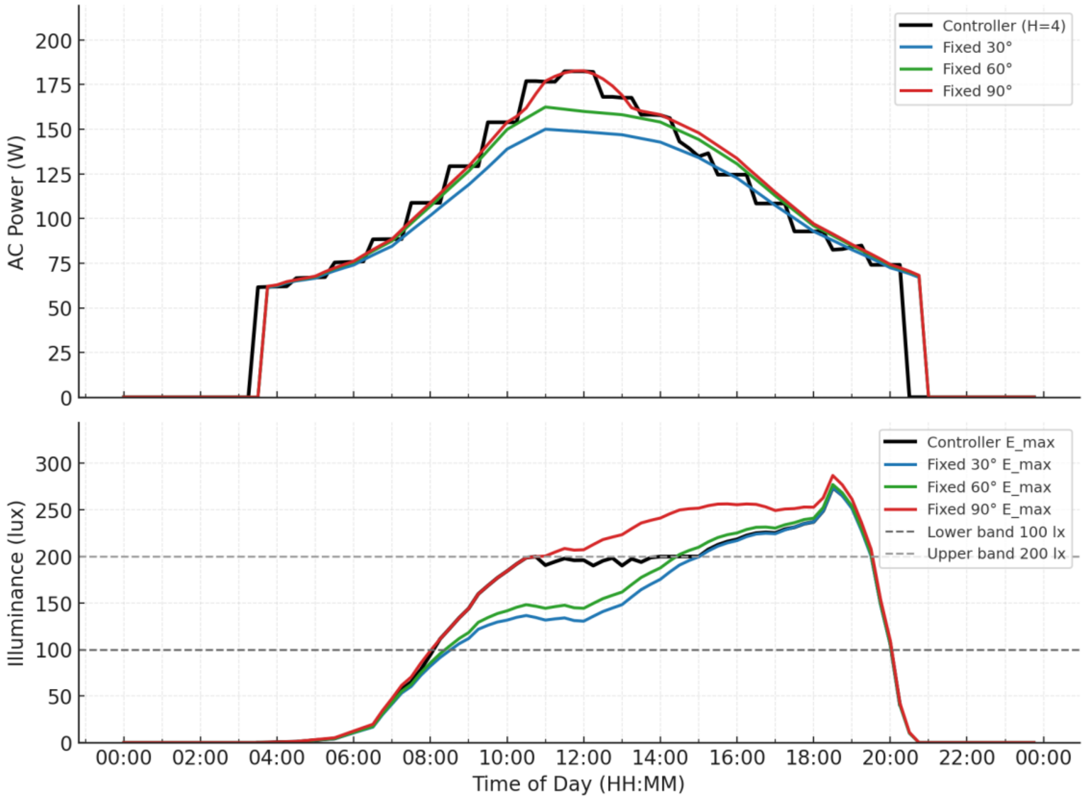

Figure 7: Comparison between MPC with H=4 vs. Fixed Angels.

The adaptive three-regime strategy (morning, midday, afternoon) proves effective in managing competing objectives across varying solar conditions. During low-irradiance periods, the controller prioritizes illuminance maintenance, while high-irradiance conditions trigger energy-focused optimization within comfort constraints. This dynamic switching reduces control conflicts and maintains consistent performance across diverse operating conditions.

The beam search optimization successfully reduces computational complexity from O(N^H) to O(K×N×H), enabling real-time implementation with solution times under 2 seconds per control step on standard hardware.

4. Conclusion

This study presented an MPC framework for PV-integrated venetian blinds that successfully addresses the fundamental trade-off between visual comfort and energy generation. The key finding is that the H=4 predictive controller maintained indoor illuminance within the 100–200 lux comfort band while matching the energy generation of optimal static configurations. Compared to myopic control, the predictive approach also significantly reduced actuator oscillations and illuminance variance, demonstrating the clear benefit of an extended prediction horizon. The methodology, which coupled physics-based models with an efficient beam search optimization, proved to be a practical framework for real-time smart façade control. The results indicate that this predictive strategy can eliminate the traditional compromise between energy harvesting and occupant comfort in BIPV systems, with modest computational needs suggesting feasibility for commercial deployment. While this evaluation focused on a single zone, future research should address multi-zone coordination, weather uncertainty, and long-term performance validation, along with integration into building energy management systems. This work positions predictive control as an enabling technology for the next generation of adaptive, energy-positive building envelopes.

5. Nomenclature

α	Solar altitude angle (°)	h	Future time step index
α_{proj}	Projected solar altitude angle (°)	J	Cost function at time t
β	Slat tilt angle relative to horizontal (°)	K	Number of top trajectories in beam search
γ	Solar azimuth angle (°)	N	Number of candidate angles per step
γ_f	Facade azimuth angle (°)	P	Photovoltaic power (W)
$\Delta\gamma$	Relative azimuth between sun and façade (°)	p	Slat pitch (m)

$\Delta\theta_{t+h}$	Slat angle change rate	$POA_{diffuse}$	Diffuse component of plane-of-array irradiance (W/m²)
Δ_{max}	Maximum allowable slat rotation per control interval	POA_{direct}	Direct component of plane-of-array irradiance (W/m²)
ε	Small numerical constant for robustness	POA_{ground}	Ground-reflected component of plane-of-array irradiance (W/m²)
θ	Slat angle relative to window plane (°)	$\mathrm{POA_{total}}$	Total plane-of-array irradiance (W/m²)
Θ_i	Angle of incidence (°)	t	Time (s)
Θ_z	Solar zenith angle (°)	w	Slat width (m)
ρ	Ground albedo (reflectance)	W_1	Weighting factor for PV power generation
$\mathrm{D(E_{t+h})}$	Illuminance deviation penalty function	W_2	Weighting factor for illuminance comfort
E	Indoor illuminance (lux)	W_3	Weighting factor for actuator smoothness
G	Global horizontal irradiance (W/m²)		
G_b	Beam (direct) normal irradiance (W/m²)		
G_d	Diffuse horizontal irradiance (W/m²)		
H	Prediction horizon (steps)		

6. Acknowledgments

The authors would like to express their sincere appreciation to the project developers of OPTIX – Optimising Positive-Energy Districts through Interoperable Digital Platforms (Project No. P2024-02859) for their valuable insights and contributions. The authors also gratefully acknowledge the support of GeoCoHorT – Geothermal Community Heat Technology and Transfer, whose financial assistance made possible the conference attendance and presentation of this study. This work has been supported by the GEOTHERMICA and JPP Smart Energy Systems Joint Call, co-funded by the Swedish Energy Agency (Project No. 451).

7. References

Akbari Paydar, M. 2020. Optimum design of building integrated PV module as a movable shading device. Sustainable Cities and Society, 62, 102368. http://dx.doi.org/10.1016/j.scs.2020.102368

Kirimtat, A., Tasgetiren, M.F., Brida, P. ,Krejcar, O. 2022. Control of PV integrated shading devices in buildings: A review. Building and Environment, 214, 108961. http://dx.doi.org/10.1016/j.buildenv.2022.108961

Liu, J., Bi, G., Gao, G. ,Zhao, L. 2023. Optimal design method for photovoltaic shading devices (PVSDs) by combining geometric optimization and adaptive control model. Journal of Building Engineering, 69, 106101. http://dx.doi.org/10.1016/j.jobe.2023.106101